Journal of Materials Chemistry A

ARTICLE

Structural Impact of Zn-insertion into Monoclinic $V_2(PO_4)_3$: Implications for Zn-ion Batteries

Min Je Park,[a] Hooman Yaghoobnejad Asl,[a] Soosairaj Therese[b] and Arumugam Manthiram*[a]

Received 00th January 20xx,
Accepted 00th January 20xx

DOI: 10.1039/x0xx00000x

www.rsc.org/

Zinc-ion battery (ZIB) has been a system of particular interest in the research community as a possible alternative to lithium-ion batteries (LIB), and much work has been devoted in finding a suitable host material. In this article, monoclinic $V_2(PO_4)_3$ is investigated as a host material for reversible insertion of Zn^{2+}. Initial chemical assessment *via* a facile microwave-assisted chemical insertion method indicates the possibility of Zn^{2+} insertion into the host. Electrochemical assessment, however, exhibits a significant capacity fade. In-depth analysis on the average and local structure of $Li_3V_2(PO_4)_3$, the empty host $V_2(PO_4)_3$, and the Zn-inserted $V_2(PO_4)_3$ reveals that heavy distortion is induced upon Zn^{2+} insertion into the $V_2(PO_4)_3$ framework, which is believed to be a result of a strong host-guest interaction jeopardizing the structural integrity. This is further supported by the dissolution of most of the material during the chemical oxidation of the Zn-inserted $V_2(PO_4)_3$. The underlying structural inadequacy poses difficulties for monoclinic $V_2(PO_4)_3$ to be a viable reversible host for Zn-ion batteries. This work suggests that not only the electrostatic repulsions of multivalent ions in a structure during diffusion, but also the structural stability of the host upon insertion of multivalent ions, must be considered for a better design of suitable host materials for multivalent-ion batteries.

Introduction

With precipitous growth in portable electronics and ever-increasing interest in large-scale systems, such as grid storage and electric vehicles, research into systems beyond the Li-ion battery (LIB) technology has incited much interest.[1–4] Among the various battery systems pursued, zinc-ion battery (ZIB) system is investigated as a potential alternative to LIBs. The ZIB system is attractive since zinc metal can be used as the anode, unlike in a LIB where the use of lithium-metal anode leads to safety hazards. Also, zinc metal is considerably lower in cost than lithium due to its higher abundance and environmental benignity. Although relatively high in reduction potential (E^0 = ~ −0.76 V *vs.* standard hydrogen electrode), a high gravimetric (820 mA h g^{-1}) and volumetric capacity (5853 mA h cm^{-3}) can be attained due to the divalent nature of the Zn ions involving two electron transfer per ion.[5,6]

By virtue of its relatively low reducing power and passivation, Zn metallic anode allows the use of aqueous electrolytes in ZIB systems. While the use of aqueous electrolytes is highly desired for the obvious reasons of abundance, cost, safety, and high dielectric constant, it can heavily obscure the true nature of the insertion chemistry of multivalent ions. This is especially the case with Zn^{2+} ions, as maintaining a relatively high concentration of Zn^{2+} in the electrolyte (0.1 to 1.0 M) requires acidic pH levels due to the low solubility of the $Zn(OH)_2$ in water (K_{sp} = 5 × 10^{-17}). Therefore, the electrolyte may merely serve as a source of H^+ cations, which can be inserted preferably into the cathode host structure if it has the Lewis basic character (normally the case for oxidic and oxo-polyanionic hosts). For example, a study on an ε-MnO_2 cathode material in aqueous Zn-ion battery revealed that the co-insertion of H^+ and Zn^{2+} is responsible for the discharge capacity, and at a high rate of 6.5C, more than 80 % of the capacity was due to H^+ insertion.[7] In a battery, such an occurrence is not necessarily unwanted, as it provides lower cost cell designs as well as fast electrochemical kinetics. However, this does not help battery scientists to achieve a deeper understanding of actual mechanisms involving multivalent-ion insertion and solid-state diffusion. Seeking for a clear insight would be critical when the use of non-aqueous electrolytes is a must, as in high-voltage ZIBs operating in a region beyond the electrochemical stability of the aqueous electrolyte, or—in a broader sense—in other multivalent-ion batteries (*e.g.*, Mg, Ca, and Al) due to the incompatibility of their respective metallic anodes with aqueous electrolytes.

Research efforts to search for suitable cathode host materials for ZIBs have been growing to date. Investigation into close-packed structures like the spinel λ-MnO_2—inspired by its use as a cathode for LIBs—has shown that electrostatic repulsion of the divalent ions like Zn^{2+} or Mg^{2+} may be too high,

[a] *Materials Science and Engineering Program & Texas Materials Institute, The University of Texas at Austin, Austin, Texas 78712, USA. E-mail: manth@austin.utexas.edu*
[b] *Department of Chemistry and Chemical Technology, Bronx Community College, Bronx, New York 10453, USA.*
† Electronic Supplementary Information (ESI) available: Chemical, electrochemical and structural analyses. See DOI: 10.1039/x0xx00000x

preventing their diffusion within the structure unlike Li^+.[8,9] In this regard, polyanionic materials with an open-framework structure could be more favorable as a host for multivalent ions, such as Mg^{2+}, Zn^{2+}, and Al^{3+}.

Ever since the reports of NASICON (**Na** **s**uper-**i**onic **con**ductor) structure—a polyanionic material—as a reversible host for electrochemical insertion of alkali ions (Li^+, Na^+),[10–12] extensive research has been conducted on its use as a cathode material for both lithium- and sodium-ion batteries.[13–15] There are many advantages associated with this structure, including chemical stability that allows long cycle life as a Li^+ and Na^+ host framework. The key advantage of the NASICON structure is—as the name suggests—the superior alkali ion conducting properties, owing to the large interstitial cavities created by highly covalent three-dimensional framework that allows relatively weak interactions between the cations in those sites and itself.[16] Among the vast selection of compositions available, vanadium phosphates ($A_xV_2(PO_4)_3$, A = Li, Na) have been of particular interest due to their relatively high discharge voltage ($Na_xV_2(PO_4)_3$ with 3.4 V *vs.* Na^+/Na[17] for x = 3 and $Li_xV_2(PO_4)_3$ with ~ 3.6, 3.7, 4.1 and 4.6 V *vs.* Li^+/Li,[13,18] respectively, for x = 3.0, 2.5, 2.0, and 1.0) and high theoretical capacity ($Na_3V_2(PO_4)_3$ with 118 mA h g^{-1} for two Na^+ extraction and $Li_3V_2(PO_4)_3$ with 197 mA h g^{-1} for three Li^+ extraction). Therefore, the $V_2(PO_4)_3$ host family have been considered as a natural choice for studying the insertion of multivalent cations.

This work attempts to reveal the true nature of Zn^{2+} interaction with the ionic conductor $V_2(PO_4)_3$ framework, free from any possible source of insertion interference. Thus far, de-sodiated $NaV_2(PO_4)_3$ obtained from $Na_3V_2(PO_4)_3$, which adopts the rhombohedral structure, has been investigated as a cathode host for multivalent-ion battery systems in aqueous (Zn, Al),[19–21] and non-aqueous (Mg) electrolytes.[22–24] Based on the abovementioned argument, it can be inferred that for a host material that can accommodate H^+ as the charge balancing cation, which is the case for $V_2(PO_4)_3$ framework,[25] insertion of much smaller monovalent H^+ cations would be preferred over Zn^{2+} or Al^{3+}. Furthermore, preferred insertion of monovalent cations like Na^+ over more charge-dense multivalent ions in $NaV_2(PO_4)_3$ is also evident in the Mg-Na hybrid battery work.[22,23] Moreover, extraction of only two Na^+ in $Na_3V_2(PO_4)_3$ is possible, with the third Na^+ remaining inaccessible even in a strong oxidizing environment, employing both conventional chemical and electrochemical methods.[26–28] On the other hand, all of the cations can be extracted from $Li_3V_2(PO_4)_3$, which crystallizes in the monoclinic structure, to yield an empty host structure of $V_2(PO_4)_3$,[29] allowing us to focus only on the interaction of the guest Zn^{2+} ion and the host framework.

Thus, we investigate here the feasibility of monoclinic $V_2(PO_4)_3$ framework as a reversible host for Zn-ion insertion and de-insertion by coupling chemical and electrochemical methods for the first time. Monoclinic $V_2(PO_4)_3$ framework has only been investigated as a host for Mg-ions to the best of our knowledge,[30] although the results suggest more evidence is required to support that the inserting cation is Mg^{2+}.[1,31] The possibility of Zn-ion insertion into the structure was first studied *via* the microwave-assisted chemical insertion method proposed by our group,[32–34] which also provided gram-scale amounts of powdered sample suitable for further structural analyses. Electrochemical Zn-ion insertion and de-insertion into the host, however, leads to extensive capacity fade. For a better understanding of the phenomenon, atomic-level structural studies on $V_2(PO_4)_3$ achieved by chemical oxidation and Zn-inserted $V_2(PO_4)_3$ obtained by the facile microwave insertion were conducted. Based on the structural analyses, we are demonstrating severe bond-strain in the host induced as a result of Zn^{2+} reductive insertion, which is believed to be due to the strong electrostatic interaction between the inserted Zn^{2+} ions and the $V_2(PO_4)_3$ host framework. From the observation that most of the material dissolved during chemical removal of Zn^{2+} from Zn-inserted $V_2(PO_4)_3$, it is believed that the structural integrity of the host is lost upon insertion of Zn^{2+} that translates into the capacity loss. The results of this study are expected to provide insight for the battery community to consider appropriate materials design strategies to minimize the extent of or otherwise suppress the multivalent cation-host interactions for stable performance of multivalent batteries.

Experimental

Synthesis of $Li_3V_2(PO_4)_3$

Precursor for the $Li_3V_2(PO_4)_3$ was synthesized *via* a sol-gel method. V_2O_5 (1.82 g, Sigma Aldrich, 99.6+%), and $C_2H_2O_4.2H_2O$ (3.78 g, Fisher Scientific, 99.5 %) in 1 : 3 mole ratio were added to 50 mL of deionized water (DIW) and heated at 80 °C, while stirring to dissolve the V_2O_5. Once a clear blue solution was formed, stoichiometric amounts of $NH_4H_2PO_4$ (3.45 g, Fisher Scientific, ≥ 98.0 %) and $LiOH.H_2O$ (1.26 g, Fisher Scientific, ≥ 98 %) were added to the solution and continuously heated while stirring, until the solution was almost dry. The remaining solution was then further dried in a vacuum oven at ~ 80 °C to remove the moisture completely. The dry precursor powder was collected and heated under Ar at 350 °C for 6 h to remove all the ammonia and moisture. After this first heating step, the intermediate powder was collected and re-ground before submitting to a second thermal treatment at 800 °C for 12 h under Ar to obtain the final product.

Preparation of $V_2(PO_4)_3$ powder *via* Chemical Oxidation

De-lithiation of $Li_3V_2(PO_4)_3$ was carried out by stirring 1.00 g of the powder in 50 mL of acetonitrile (AN, Sigma Aldrich, ≥ 99.8 %) with 3.3 equivalent moles of NO_2BF_4 (1.08 g, BeanTown Chemicals, 96 %) at room temperature, while keeping under N_2 atmosphere by a Schlenk line. After oxidation, the powder was rinsed with fresh AN to remove any remaining NO_2BF_4 and filtered with a centrifuge. The filtered powder was dried in a vacuum oven maintained at ~ 80 °C.

Microwave-assisted Chemical Insertion for Zn^{2+} Insertion

Microwave-assisted insertion of Zn^{2+} ions into the chemically prepared $V_2(PO_4)_3$ powder was conducted with an Anton Paar Monowave 300 microwave instrument under ambient conditions. First, an appropriate amount of ZnI_2 (0.12 g, Sigma

Aldrich, ≥ 98 %) was added into a 30 mL borosilicate glass reaction vessel filled with 10 mL of N,N-dimethylformamide (DMF) (Fisher Scientific, ≥ 99.8 %) inside an Ar-filled glovebox. The mixture was stirred to dissolve the salt. Then, 0.10 g of the $V_2(PO_4)_3$ powder was added—1.5 : 1 mole ratio to the iodide—into the DMF solution. The reaction vessel was then inserted into the instrument for microwave irradiation at various temperatures and times set on the instrument.

Preparation of $V_2(PO_4)_3$ Electrodes *via* Electrochemical Oxidation

Cathodes for electrochemical testing were prepared through a number of steps. First, 0.50 g of $Li_3V_2(PO_4)_3$ powder, 0.11 g of Super P conductive carbon, and 1.07 g of 10 wt. % polyvinylidene fluoride (PVdF) binder dissolved in N-methyl-2-pyrrolidone (NMP) were mixed with an additional 1.5 mL of NMP (weight ratio of 70 : 15 : 15) to obtain a homogeneous slurry. The slurry was then coated onto a Toray carbon paper current collector (TGP-H-120, Fuel Cell Earth) and was dried in a vacuum oven before punching out discs with diameters of 3/8 of an inch for electrochemical cells. The active material loading was typically in the range of 5 ~ 8 mg cm^{-2}. In order to obtain electrodes with the $V_2(PO_4)_3$ active material, electrochemical oxidation of the $Li_3V_2(PO_4)_3$ cathode was carried out with Swagelok cells, which were assembled in an Ar-filled glovebox. In each cell, the prepared electrode, a Li metal foil, and a glass fiber separator and a polypropylene separator were used, respectively, as the cathode, the anode, and the separator. The electrolyte used for the de-lithiation step was 100 μL of 1.0 M $LiPF_6$ in ethylene carbonate (EC) and ethyl methyl carbonate (EMC) mixture (EC : EMC = 3 : 7 by weight) with 2 wt. % vinylene carbonate (VC) added as an additive. After assembly, linear sweep voltammetry (LSV) was conducted on the Swagelok cell, scanning the potential up to 5.0 V at a scan rate of 20 μV s^{-1} to ensure the removal of all the Li^+ from the cathode structure. The charged cell was then disassembled inside an Ar-filled glovebox, and the retrieved cathode was washed with dimethyl carbonate (DMC) to remove any residual electrolyte before storing inside the glovebox.

Electrochemical Analysis of $V_2(PO_4)_3$ in Non-aqueous Zn-ion Set-up

Zn-ion electrochemical testing was performed by constructing a custom-made two-electrode flooded cell. To prepare the cathode side, the prepared $V_2(PO_4)_3$ electrode disc was affixed to a graphite rod, which served as the current collector, using a conductive paste consisting of Super P and PVdF dispersed in NMP. This was left in a vacuum oven to remove all of the NMP. Zn metal foil was used as a counter and reference electrode. For both the cathode and anode, Inconel wire was used as the external wire. The flooded cell was assembled in an Ar-filled glovebox, in which the cathode and the anode components were placed in a sealed glass test tube, and the test tube was flooded with 1 mL of 0.3 M $Zn(CF_3SO_3)_2$ in propionitrile (PN) electrolyte. Cyclic voltammetry (CV) and galvanostatic cycling were carried out with a VMP3 Bio-logic potentiostat instrument.

Material Characterization

Structural information on the materials was obtained with a Rigaku Miniflex 600 X-ray diffractometer equipped with Cu Kα radiation (λ = 1.5404 Å) source. The XRD patterns used for structural refinement was obtained by scanning the 2θ angular range from 10 to 90 ° in steps of 0.02 ° for 2.7 s dwell time at each step. Rietveld refinement was performed on the powder XRD patterns using the GSAS-II software.[35] For the Zn-inserted sample, the position of zinc was first located by inspecting the calculated difference Fourier map between the observed and calculated structure factors. Subsequently, the site occupancy of the zinc along with the fractional coordinates of all of the atoms was released for refinement in a stepwise procedure. Wide-angle x-ray scattering measurements (WAXS) was performed with a Scintag X1 diffractometer equipped with a Mo X-ray tube (λ = 0.7107 Å). The 2θ angular region from 4 to 158 ° was scanned in 0.04 ° increments, for a dwell time of 30 s at each step (32 h total measurement time). The combination of a long exposure time along with wide angular scan range provides scattering data with a decent Q-space sampling from 0.617 to 17.35 $Å^{-1}$ and acceptable count statistics. The obtained data are suitable for the extraction of local atomic environment information through the Pair Distribution Function analysis (PDF). For this, data correction and transformation has been done with the GSAS-II software package, with the refinement of the real-space G(r) function against an atomistic model accomplished using the PDFgui software.[36]

For the oxidation state analysis following the Zn^{2+} insertion into $V_2(PO_4)_3$, the sample was dissolved in 10 mL of boiling 6 N sulfuric acid in a sealed three-neck flask under continuous Ar purge to avoid aerial vanadium oxidation. After complete dissolution, the solution was cooled down to room temperature and the titration was conducted by adding increments of 0.1 N $KMnO_4$ without exposing the solution to air. The potential of the solution was measured with an inert Pt working electrode *vs.* saturated Ag/AgCl reference.

Scanning electron microscope (SEM) images were captured with a JEOL JSM-5610 equipped with an energy dispersive X-ray spectrometer (EDS), which was also used for elemental analysis before conducting inductively coupled plasma (ICP) analysis with a Varian 715-ES ICP optical emission spectrometer.

Results and discussion

Synthesis of $Li_3V_2(PO_4)_3$ and Preparation of $V_2(PO_4)_3$ *via* Chemical Oxidation

The observed powder XRD pattern of the as-synthesized $Li_3V_2(PO_4)_3$ is presented along with the calculated pattern in Fig. 1a. Refinement for the lattice parameters using the phase data of $Li_3V_2(PO_4)_3$ reference pattern (JCPDS No. 72-7074, monoclinic, space group: $P2_1/n$) indicates that all of the diffraction peaks could be indexed to monoclinic $Li_3V_2(PO_4)_3$. Also, the calculated unit cell volume of 888.4 $Å^3$ is in close agreement with that of the reference (~ 890 $Å^3$), verifying that a pure material was synthesized. Sharp and intense diffraction

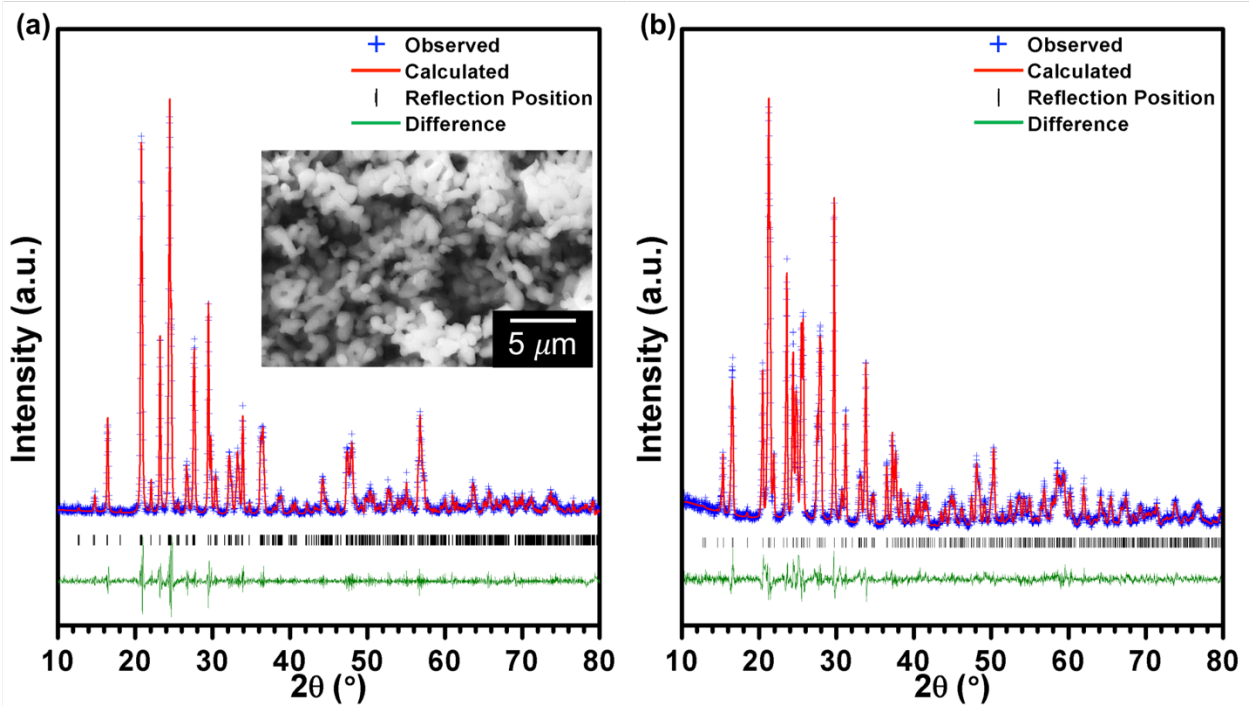

Fig. 1 Refined powder diffraction pattern of (a) the as-synthesized $Li_3V_2(PO_4)_3$ (with accompanying SEM image) and (b) $V_2(PO_4)_3$ prepared *via* chemical oxidation.

peaks signify good crystallinity of the synthesized material. The SEM image (inset, Fig. 1a) shows that the particles are homogenous, granular in shape, and of 1 – 2 μm in size on average. Elemental ratio of Li and V from ICP measurement was determined to be Li : V = 2.99 : 2.00, further confirming the synthesis of $Li_3V_2(PO_4)_3$.

In order to discern whether topotactic insertion of Zn^{2+} into this material is possible, the as-synthesized $Li_3V_2(PO_4)_3$—populated with Li^+—was first chemically oxidized to remove the Li^+ to obtain a vacant host material. Since the extraction potential of the 3rd Li^+ is ~ 4.6 V *vs.* Li^+/Li, a strong oxidizing agent NO_2BF_4 with a high redox potential of ~ 5.1 V *vs.* Li^+/Li was used.[37,38] To ensure extraction of all the three Li^+ ions from the structure to obtain the $V_2(PO_4)_3$ host, excess NO_2BF_4 (3.3 equivalent moles) was added to the AN and the reaction was left to run for 24 h. Rietveld refinement was performed on the diffraction pattern of the collected powder using the reference phase data of $V_2(PO_4)_3$ (JCPDS No. 72-7077, monoclinic, space group: $P2_1/n$) and the results are presented in Fig. 1b. Refined lattice parameters and atomic positions are listed in Table S1†. It is to be noted that the Rietveld-derived unit cell volume for the maximally delithiated vanadium phosphate is slightly smaller than those reported earlier (813.09(6) Å^3 vs. ~ 830 Å^3). This is believed to be due to some Li^+ remaining in the structure as determined *via* the ICP analysis (Li : V = 0.25 : 2.00). Nevertheless, the calculated diffraction pattern is in good agreement with the observed one with good refinement statistics (Table S1†). Furthermore, the bond-lengths and angles for the V and P centers match well with, respectively, the expected octahedral and tetrahedral coordination environments following an unconstrained refinement of the atomic coordinates. The calculated bond valence sum (BVS) on the two V centers are +4.83 and +4.01, resulting in an average oxidation state of +4.42, which is close to +4.37 expected in $Li_{0.25}V_2(PO_4)_3$. The calculated BVS on the three P centers are +4.92, +4.97, and +4.98, respectively, for the P1, P2 and P3 atoms, all in agreement with the expected oxidation state of +5. All in all, the crystallographic results are showing that the phase of the powder after chemical oxidation can be assigned to delithiated monoclinic $V_2(PO_4)_3$ and henceforth will be referred to as $V_2(PO_4)_3$.

Microwave-assisted Chemical Insertion of Zn^{2+} into $V_2(PO_4)_3$

The feasibility of monoclinic $V_2(PO_4)_3$ structure as a host material for Zn^{2+} insertion was assessed by attempting microwave-assisted chemical reduction on the $V_2(PO_4)_3$ obtained after the chemical oxidation step. ZnI_2 was selected as the reducing agent for this process in which I^- would reduce the transition metal center while the Zn^{2+} would be intercalated into the structure as the charge balancing cation if topotactic insertion can occur. Iodide is a known mild reducing agent and has been used for chemical insertion of lithium into various lithium-ion cathode materials with a redox potential of ~ 3 V *vs.* Li^+/Li[39,40] and hence was deemed suitable to reduce the V in $V_2(PO_4)_3$.

At a temperature of 140 °C, microwave irradiation of mere 10 min resulted in a significant difference in the structure of the material as presented in Fig. 2. Since Zn^{2+} insertion into monoclinic $V_2(PO_4)_3$ has not been attempted previously, no prior structural information is available regarding this phase. Hence, the diffraction pattern of the as-synthesized $Li_3V_2(PO_4)_3$ is also presented for visual comparison. Noticeable peak shifts to lower 2θ angles and more importantly, the resemblance of the overall pattern after microwave irradiation to that of the $Li_3V_2(PO_4)_3$ was observed, suggesting V reduction with Zn^{2+}

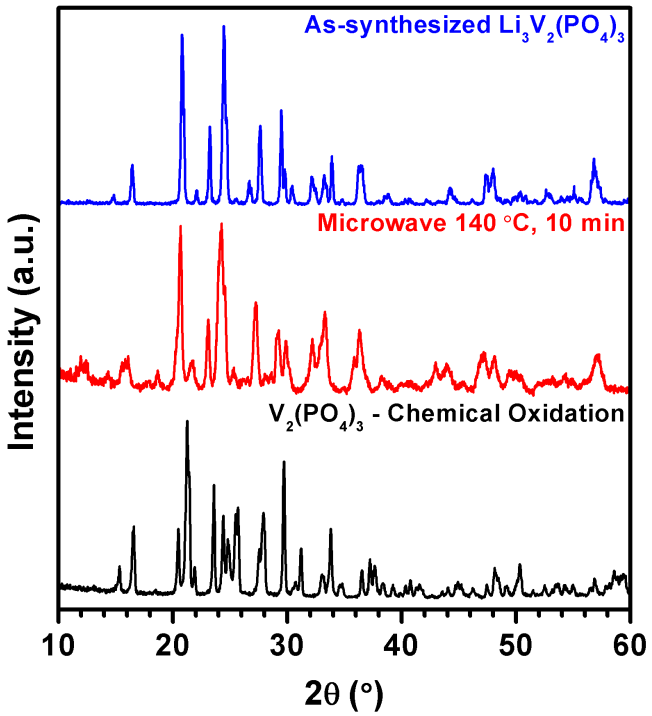

Fig. 2 XRD patterns of $V_2(PO_4)_3$ before microwave irradiation and after microwave irradiation with ZnI_2 at 140 °C for 10 min, and as-synthesized $Li_3V_2(PO_4)_3$ for a comparison.

insertion into $V_2(PO_4)_3$ host while maintaining the same framework. Nonetheless, there are detectable changes such as peak broadening and rearrangement of peak intensities following the reduction. A detailed Redox titration with $KMnO_4$ oxidant signified a change in the average oxidation state of V from +4.42 to +3.12, confirming that V centers were reduced by the combined action of iodide and microwave irradiation (Fig. S1†). Elemental analysis conducted determined that 1.07 Zn per formula unit is present in the sample, verifying that reduction of V centers is accompanied by the insertion of Zn^{2+} into the structure. Even when all of the Zn in the sample is assumed to be in the $V_2(PO_4)_3$ structure, there is a difference of 0.62 electrons per formula unit. This discrepancy may be due to side reactions that occur during the microwave irradiation and further investigation is required in this regard. Iodide reduction was also performed at lower temperatures of 50 °C and 80 °C at various time intervals of up to 3 h to discern whether facile Zn^{2+} insertion is also possible at lower temperatures. No distinct difference in the structure of the material was observed as shown on Fig. S2†, which suggests that Zn^{2+} insertion is kinetically limited and much longer times are required at lower temperatures for a similar degree of Zn^{2+} insertion to that at 140 °C. This is not surprising since the prepared material consists of bulk particles.

Electrochemical Analysis of $V_2(PO_4)_3$ in a Non-aqueous Zn-ion Set-up

Having identified that $V_2(PO_4)_3$ can act as a host for Zn ions, electrochemical Zn-ion insertion and de-insertion was attempted to assess the reversibility of the host material. To prepare electrodes of the empty host $V_2(PO_4)_3$, $Li_3V_2(PO_4)_3$ electrodes were prepared and electrochemically charged in Li-ion cells by conducting LSV up to 5.0 V *vs.* Li^+/Li to ensure complete Li extraction (Fig. S3a†). This was verified by running a galvanostatic discharge on the charged electrode in the same cell (Fig. S3b†). The discharge profile exhibits a sloping curve, indicative of the solid-solution behavior upon re-insertion of Li with a similar discharge capacity as reported.[13,41]

From the CV performed on the electrochemically prepared $V_2(PO_4)_3$ at a scan rate of 50 μV s^{-1}, hardly any reduction or oxidation was observable at room temperature (Fig. S4†). This is considered to be due to the poor diffusion kinetics of the Zn^{2+} in the bulk $V_2(PO_4)_3$ particles. To overcome this limitation, all electrochemical tests were conducted at 80 °C, which unavoidably promoted the side reactions, as evident by the evolution of current toward the anodic vertex potentials during the CV of the blank system (Toray paper + graphite rod) (black, Fig. 3a) within the voltage window of 0.5 – 1.9 V *vs.* Zn^{2+}/Zn. In spite of this, the CV of $V_2(PO_4)_3$ (red, Fig. 3a) indicates an obvious electrochemical reduction and oxidation. The potential of an assembled cell was swept initially from the open-circuit voltage of 1.56 V toward the cathodic vertex at 0.5 V, leading to a broad current step, indicating Zn^{2+} insertion. On the contrary, the CV exhibits a broad peak during the anodic scan in which the peak current is reached at the limiting potential of 1.9 V. From the broadness of the cathodic and anodic behaviors, it can be deduced that the Zn^{2+} diffusion into and out of the host structure is extremely impeded even at 80 °C.

It is worth mentioning that complete Li^+ removal from monoclinic $Li_3V_2(PO_4)_3$ structure is crucial for an unambiguous understanding of the electrochemical insertion and extraction behavior of Zn^{2+} to avoid false interpretation when coupling the cathode with the Zn anode. Zn^{2+} insertion into monoclinic $LiV_2(PO_4)_3$—two Li^+ extracted from the structure—follows a similar trend as that of the empty host structure. However, the first extraction is accompanied with a strong, relatively narrow anodic peak at ~ 1.73 V (Fig. S5a†), which is completely absent from the $V_2(PO_4)_3$ host. The CV conducted on monoclinic $Li_3V_2(PO_4)_3$ in the same Zn-ion electrochemical set-up starting from the anodic scan shows only the removal of the first and incomplete removal of the second Li (Fig. S5b†). As a result, the 1.9 V anodic potential cut-off applied is not sufficient to extract the third Li, which resides in the most stable crystallographic site in $Li_3V_2(PO_4)_3$. Therefore, one can conclude that the sharp anodic peak is due to the internal site exchange of Zn^{2+} and Li^+ ions, with a concomitant removal of the Li from $Zn_xLiV_2(PO_4)_3$, similar to a hybrid Zn-Li cell. Elemental ratio of Li and Z versus V obtained via ICP measurements of the $LiV_2(PO_4)_3$ electrode after the first reduction illustrate the insertion of Zn ions, and after the subsequent oxidation, both the Li and Zn contents decrease, further supporting concomitant removal of both ions (Table S2†). In the following cycles, this anodic peak fades as more and more Li is removed from the host, and eventually the electrochemical behavior of the cathode becomes similar to that of $V_2(PO_4)_3$.

Successive cyclic voltammograms plotted on Fig. 3a exhibit similar reduction and oxidation behavior but with lower charge

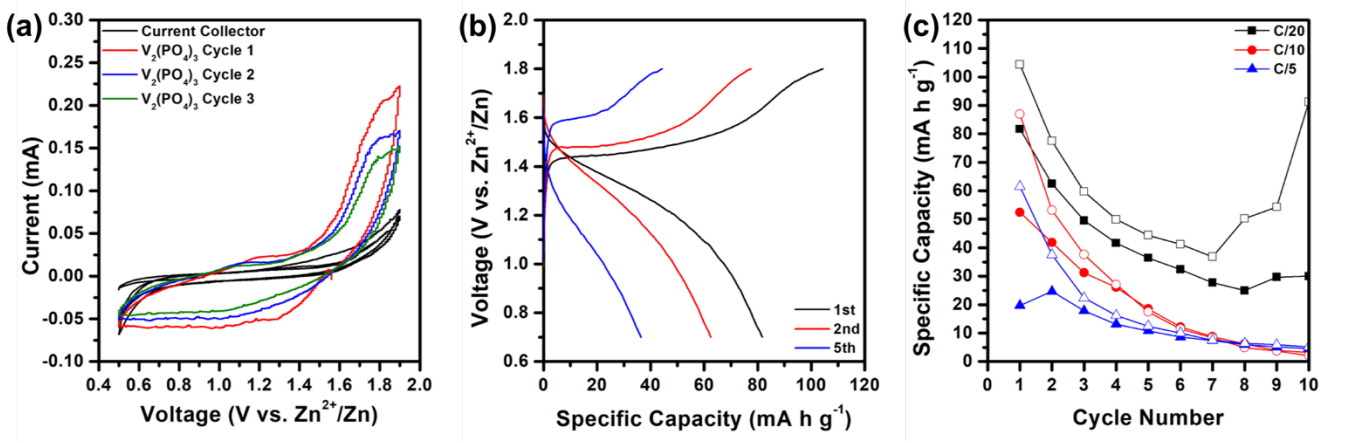

Fig. 3 (a) CV curves of the blank system (Toray paper + graphite rod) and $V_2(PO_4)_3$, (b) charge and discharge curves at C/20 rate, and (c) galvanostatic cycling performance of $V_2(PO_4)_3$ at various C rates.

transfer per cycle, indicating poor electrochemical reversibility of $V_2(PO_4)_3$. This is also reflected on the charge-discharge curves at a rate of C/20 after different numbers of cycles and galvanostatic cycling at various C rates (Fig. 3b and c). The first cycle Zn^{2+} insertion into $V_2(PO_4)_3$ host at a C rate of C/20 yields a specific capacity of 82 mA h g^{-1} at a cut-off potential of 0.7 V, corresponding to the insertion of ~ 1.2 e^- (~ 0.6 Zn^{2+}) into the formula unit at an average potential of 1.2 V. A quarter of this capacity is lost in the second cycle and by the fifth cycle, only ~ 45 % of the capacity is retained. At higher C rates of C/10 and C/5, this trend is more pronounced. The significant capacity loss upon successive cycling indicates the irreversibility of the thermodynamics of Zn^{2+} insertion/extraction into $V_2(PO_4)_3$ structure, even though the employed high temperature allows for the diffusion to take place.

Structural Analysis on Zn-inserted $V_2(PO_4)_3$

To unveil the underlying phenomenon contributing to the rapid capacity fade, a detailed structural study was conducted. However, acquiring a processable XRD pattern from an electrochemically cycled electrode can be problematic. Not only the small amount of active material on the electrode (5 ~ 6 mg

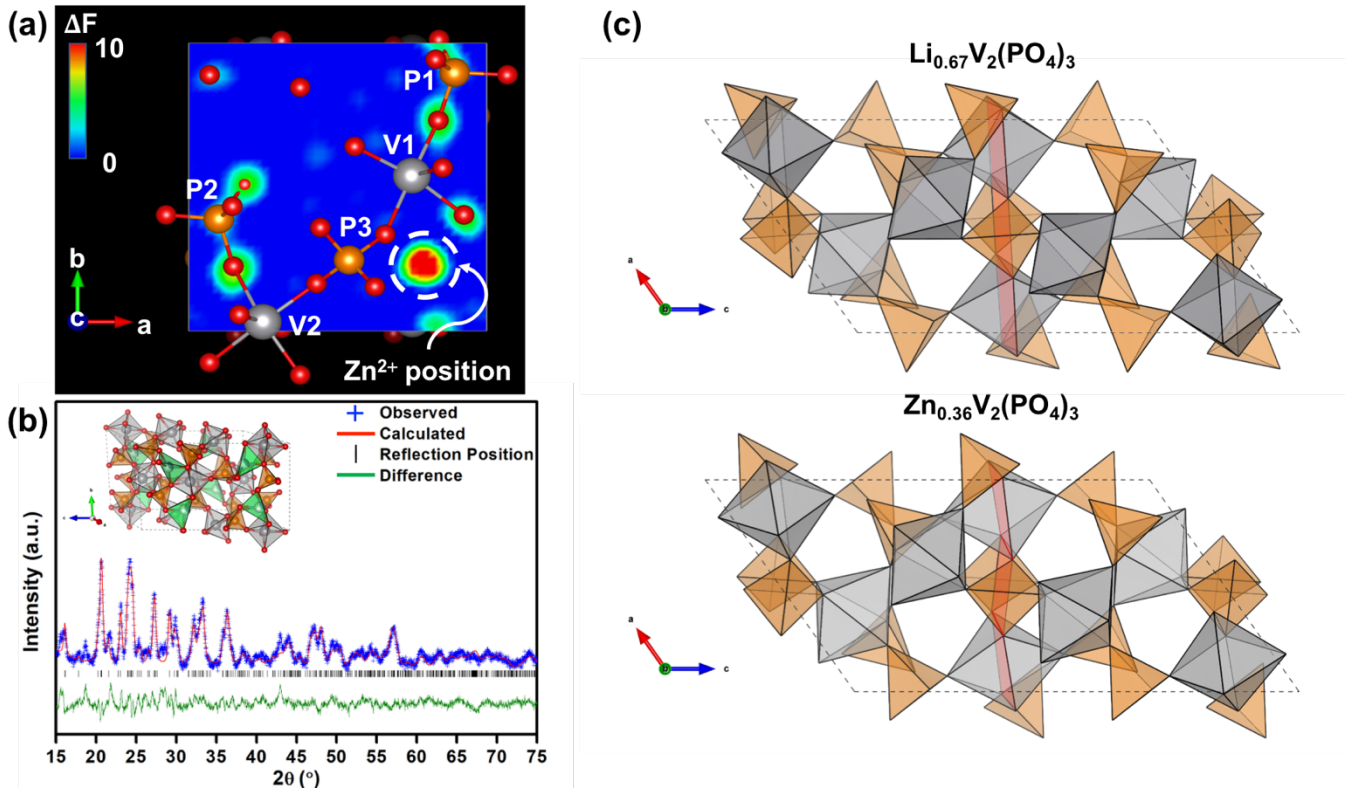

Fig. 4 (a) Difference Fourier map cross-section along [001] (z = +7.62 Å), (b) refined diffraction pattern obtained from the Rietveld refinement of Zn^{2+} inserted $V_2(PO_4)_3$ powder diffraction data, and (c) crystal structures of $Li_{0.67}V_2(PO_4)_3$ (above) and $Zn_{0.36}V_2(PO_4)_3$ (below) with the imaginary red plane highlighting the difference in the torsion angle between the two (the guest ions are eliminated from the plots for clarity).

on average), but also the introduction of high intensity peaks of the current collector (Toray paper) that overlaps with the peaks of the active material renders refinement impractical (Fig. S6†). Also, the presence of other materials including PVdF binder and Super P increases the background. Based on the resemblance of the XRD patterns of the Zn-inserted $V_2(PO_4)_3$ *via* microwave-assisted chemical insertion and electrochemical Zn^{2+} insertion as presented in Fig. S6†, it is believed that both chemical and electrochemical methods of Zn^{2+} insertion provide similar results. Hence, the powder XRD pattern of the Zn-inserted $V_2(PO_4)_3$ *via* microwave-assisted chemical insertion was refined by Rietveld method, starting from the $Li_{2.5}V_2(PO_4)_3$ crystal structure as the model. To avoid complications, the low-angle impurity peaks ($2\theta < 15$ °) introduced after microwave irradiation was excluded from the refinement process. Following the refinement of the unit cell and V, P and O fractional coordinates, a difference Fourier map was calculated by subtraction of the observed structure factor from the calculated ones for each Bragg reflection (Fig. 4a). The Fourier difference map immediately shows a high-intensity peak, with a distance of ~ 2 Å from the oxygen atoms (indicated with the dashed circle in Fig. 4a). Given the heavy nature of the Zn atom, the observed peak has been assigned as Zn, and the fractional coordinates and site occupancy factor was flagged for refinement. This reduces the full pattern weighted residuals from ~ 20 % to 16.9 % (Fig. 4b). The refined crystal structure of Zn^{2+} inserted $V_2(PO_4)_3$ *via* microwave-assisted chemical insertion is presented in the inset of Fig. 4b. An unconstrained refinement of the Zn site occupancy gives the formula as $Zn_{0.36}V_2(PO_4)_3$. Inspection of the atomic environment of the Zn indicates that the Zn^{2+} adopts a distorted tetrahedral environment at the general position 4e (inset, Fig. 4b). This is further supported by the crystal preference of the Zn^{2+} to reside in a tetrahedral environment. Furthermore, a BVS analysis gives an oxidation state of +2.04, which matches well with the formal oxidation state of the Zn^{2+} cation. The crystallographic data is presented in Table S3†.

Detailed analysis of the Zn-inserted $V_2(PO_4)_3$ crystal structure indicates that the Zn^{2+} is occupying essentially the Li(2) site in $Li_3V_2(PO_4)_3$. This is the most stable crystallographic site, as extraction of Li^+ from it requires application of a potential of ~ 4.6 V *vs.* Li^+/Li. Additionally, Zn^{2+} insertion is accompanied with a heavy distortion of the $V_2(PO_4)_3$ base structure. This is best demonstrated by the alteration of $V(1)O_6$-PO_4-$V(2)O_6$ torsion angles. For example, the V1-P3-V2 polyhedral torsion angle deviates from the 0.33 ° in the lithiated phase to 15.12 ° in the Zn-inserted $V_2(PO_4)_3$, causing buckling of the originally flat crystal planes containing the V centers (Fig. 4c). The twisting and buckling of the VO_6 polyhedral units are due to the strong Zn—O interactions that induce a significant stress on the $V_2(PO_4)_3$ host structure.

While XRD and Rietveld refinement is a powerful technique for the assessment of long-range order and average crystal structure, they provide little information regarding the local structure within a few angstrom length scales. This especially holds for the current case, where peak broadening is evident following Zn^{2+} insertion (Fig. 2). For a better understanding of the effect of insertion and extraction of the cations in the

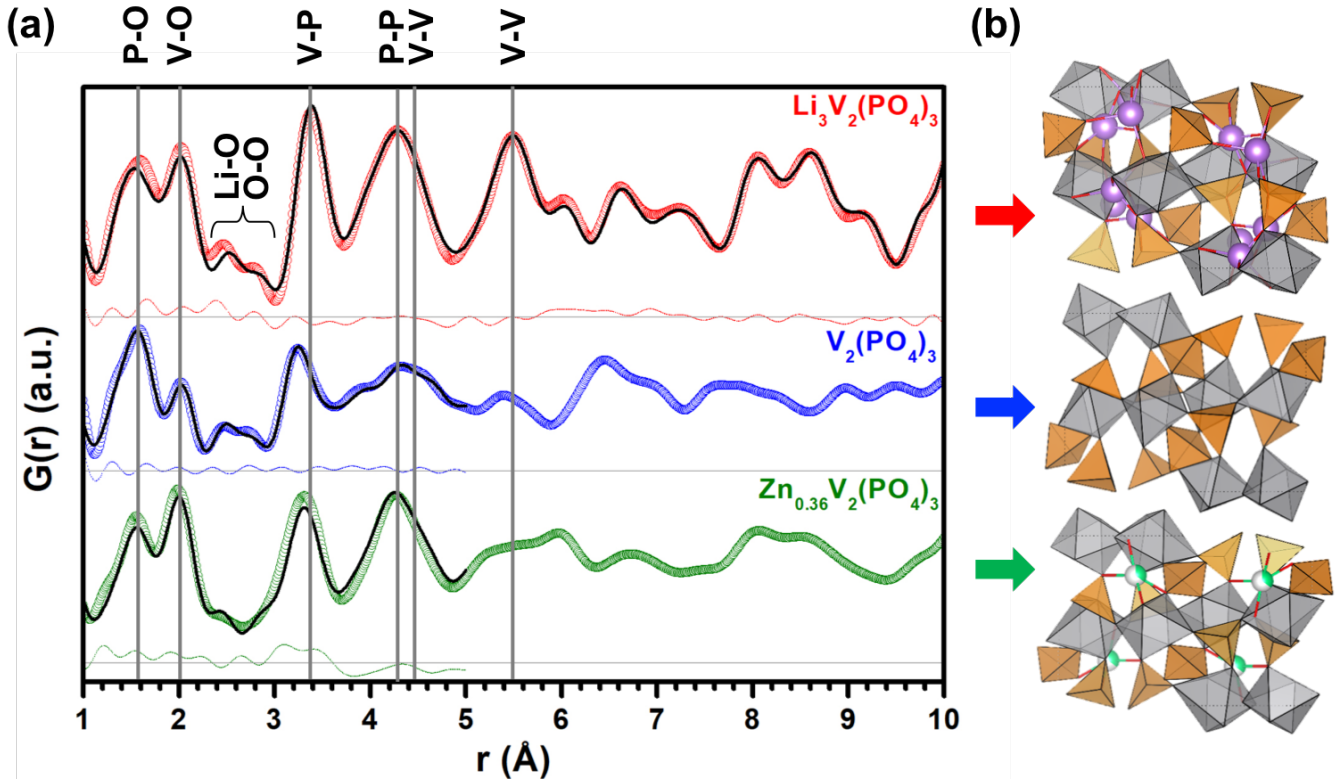

Fig. 5 The observed (open circle) and calculated (solid black line) PDF curves of $Li_3V_2(PO_4)_3$ (top), $V_2(PO_4)_3$ (middle), and $Zn_{0.36}V_2(PO_4)_3$ (bottom). The difference curve is marked with the dotted line. (b) Polyhedral view of the atomistic models used in obtaining the calculated PDF curves; Li^+: purple, Zn^{2+}: green, VO_6 octahedra: grey, PO_4 tetrahedra: orange.

monoclinic vanadium phosphate structure, the powders of $Li_3V_2(PO_4)_3$, $V_2(PO_4)_3$, and $Zn_{0.36}V_2(PO_4)_3$ were analyzed with WAXS measurement and PDF analysis (Fig. 5a). Some of the notable interatomic distance in the respective phases are marked.

The PDF plot of the $Li_3V_2(PO_4)_3$ exhibits the characteristic local structure of a highly crystalline phase with an essentially identical average and local structures. For an ordered structure like this, the radial distribution function G(r) peaks remain sharp and intense as the real-space distance r increases. Therefore, the observed G(r) can be modeled essentially with the averaged crystal structure obtained from the cif (Fig. 5b).

With respect to the local structure of the empty host $V_2(PO_4)_3$, three major differences compared to the $Li_3V_2(PO_4)_3$ phase can be identified: (1) the decrease in the probability of finding two atoms at ~ 2 Å (indicative of V—O interatomic distances), which reflects a heavy disorder in VO_6 environment as V(IV,V) is known to be stabilized by the formation of very short, covalent V—O bonds as in vanadates or vanadium pentoxide, (2) the shrinkage of the lattice due to the oxidative removal of the Li^+ ions, as exemplified by the shortening of the V—P interatomic distance (3.2 Å) compared to that in $Li_3V_2(PO_4)_3$ (3.4 Å), and (3) the decreased long-range order as the structural disorder broadens the G(r) peaks, especially toward the higher real-space distances (the PDF plots in the range of 1 – 20 Å are provided in Fig. S7†).

Inspection of the PDF curve of the Zn-inserted $V_2(PO_4)_3$ host reveals that while the local environment of the VO_6 and PO_4 polyhedral units are restored back alike to that of the $Li_3V_2(PO_4)_3$, the medium to long range order is heavily lost. For example, the sharp G(r) peak at 5.5 Å representing the V-V interatomic distance in $Li_3V_2(PO_4)_3$ is highly broadened in the Zn-inserted phase, as is the case for longer-distance atomic pairs. This corresponds with the VO_6 octahedra twisting as observed from the Rietveld refinement, because random twisting of the polyhedral units diminishes the medium- and long-range structural order in general. Therefore, it is evident that the insertion of Zn^{2+} into $V_2(PO_4)_3$ structure instigates heavy structural disorder, which is intuitively the major contributor to the capacity loss during the electrochemical cycling.

In order to test this hypothesis, we intended to study the long- and short-range structure in the $V_2(PO_4)_3$ prepared by re-oxidation of the $Zn_{0.36}V_2(PO_4)_3$ phase, to see if the Zn-induced structural strains are reversible. Zn extraction was attempted in the same manner as the preparation of $V_2(PO_4)_3$ from $Li_3V_2(PO_4)_3$, but using excess NO_2BF_4 for a much-extended time of ~ 72 h since Zn diffusion would be kinetically limited unlike Li. Within several hours of reaction, a color change from bright yellow to dark brown was evident in the reaction mixture. After the reaction, however, less than 10 % of the initial sample mass could be recovered from the mixture, while the majority of the vanadium ions were ended up in the AN solvent, as was evident from the color of the solution. This important observation suggests that the lattice stress developed in the Zn-inserted $V_2(PO_4)_3$ increases the solubility of the V species in the electrolyte by destabilizing the solid. This was also experimentally confirmed as the nitrile-based electrolyte used during the electrochemical experiments was deeply colored following a few cycles.

From the in-depth structural analysis on Zn-inserted $V_2(PO_4)_3$, we can deduce that monoclinic $V_2(PO_4)_3$ host structure is not able to accommodate the divalent Zn^{2+} in a reversible manner, being unable to withstand the stress and the deformation induced when Zn^{2+} is inserted. This key conclusion of the current study suggests that the insertion follows an essentially non-topotactic pathway, given that exclusively Zn^{2+} and $V_2(PO_4)_3$ host interaction is concerned. While this has been observed here for the monoclinic polymorph of the $V_2(PO_4)_3$ family, the finding is expected to be more or less applicable to other polyanionic hosts with non-close-packed structures due to the strong Zn–O interactions and the polyhedral connectivity deformations. Furthermore, the results obtained here call for a meticulous analysis of the electrochemical data concerning Zn^{2+} insertion; this is especially the case with aqueous electrolytes where the solvent co-insertion and/or competitor cation insertion (*e.g.*, H^+) is a possibility. A difference in electrochemical behavior may be observed for the monoclinic $V_2(PO_4)_3$ if aqueous electrolytes are used due to preferred and topotaxial H^+ insertion over Zn^{2+}, although further investigations are warranted.

Conclusions

Here, the feasibility of monoclinic $V_2(PO_4)_3$ as a reversible host for Zn-ion insertion and de-insertion was investigated both chemically and electrochemically. The ability of the host to accommodate Zn^{2+} was first confirmed *via* the facile microwave-assisted Zn^{2+} insertion using ZnI_2 as the cation source and the reducing agent. Following electrochemical study to determine the reversibility of the host structure for Zn-insertion and de-insertion indicated severe capacity fade. Detailed structural analyses on the chemically prepared $V_2(PO_4)_3$ and Zn-inserted $V_2(PO_4)_3$ was carried out for a better understanding of the capacity fade. Crystallographic analysis on the powder XRD data of Zn-inserted $V_2(PO_4)_3$ unveiled the Zn positions and the tetrahedral coordination in the crystal. Also, the distortion of the $V_2(PO_4)_3$ host structure was recognized, demonstrated by the rather large twisting and buckling of the VO_6 and PO_4 polyhedral building blocks. WAXS analysis on $Li_3V_2(PO_4)_3$, $V_2(PO_4)_3$, and $Zn_{0.36}V_2(PO_4)_3$ clarified the partial loss of the long-range order in the highly crystalline $Li_3V_2(PO_4)_3$ upon the extraction of Li^+ and the incomplete recovery of that long-range order after Zn-insertion into the empty host while leaving the host lattice in a strained state. Chemical oxidation of $Zn_{0.36}V_2(PO_4)_3$ for Zn extraction exhibited a similar color change from yellow to brown due to Zn-removal but resulted in the dissolution of > 90 % of the material, from which it can be deduced that the structural integrity is lost due to the distortion developed by Zn^{2+} insertion. To summarize, it has been shown that at the operating conditions, the capacity loss can be attributed to the host-guest interactions and structural instability of the host, rather than the diffusion kinetics and ion-trapping. Electrostatic interaction between the inserted Zn ions

and the $V_2(PO_4)_3$ host framework results in a heavy structural deformation that poses difficulties for the monoclinic $V_2(PO_4)_3$ to be a reversible host for Zn^{2+} insertion. Also, both the electrostatic repulsions encountered by the divalent-ions during diffusion and the structural instability issues must be considered in designing suitable hosts for multivalent-ion batteries.

Conflicts of interest

There are no conflicts to declare.

Acknowledgements

This work was supported by the National Science Foundation Division of Materials Research under award number 1709081 and Welch Foundation grant F-1254.

References

1 P. Canepa, G. Sai Gautam, D. C. Hannah, R. Malik, M. Liu, K. G. Gallagher, K. A. Persson and G. Ceder, *Chem. Rev.*, 2017, **117**, 4287–4341.
2 J. Muldoon, C. B. Bucur and T. Gregory, *Chem. Rev.*, 2014, **114**, 11683–11720.
3 H. D. Yoo, I. Shterenberg, Y. Gofer, G. Gershinsky, N. Pour and D. Aurbach, *Energy Environ. Sci.*, 2013, **6**, 2265–2279.
4 M. S. Whittingham, C. Siu and J. Ding, *Acc. Chem. Res.*, 2018, **51**, 258–264.
5 M. Song, H. Tan, D. Chao and H. J. Fan, *Advanced Functional Materials*, 2018, **28**, 1802564.
6 G. Fang, J. Zhou, A. Pan and S. Liang, *ACS Energy Lett.*, 2018, **3**, 2480–2501.
7 W. Sun, F. Wang, S. Hou, C. Yang, X. Fan, Z. Ma, T. Gao, F. Han, R. Hu, M. Zhu and C. Wang, *J. Am. Chem. Soc.*, 2017, **139**, 9775–9778.
8 J. C. Knight, S. Therese and A. Manthiram, *J. Mater. Chem. A*, 2015, **3**, 21077–21082.
9 J. C. Knight, S. Therese and A. Manthiram, *ACS Appl. Mater. Interfaces*, 2015, **7**, 22953–22961.
10 C. Delmas, F. Cherkaoui, A. Nadiri and P. Hagenmuller, *Materials Research Bulletin*, 1987, **22**, 631–639.
11 A. Manthiram and J. B. Goodenough, *Journal of Solid State Chemistry*, 1987, **71**, 349–360.
12 A. Manthiram and J. B. Goodenough, *Journal of Power Sources*, 1989, **26**, 403–408.
13 H. Huang, S.-C. Yin, T. Kerr, N. Taylor and L. F. Nazar, *Advanced Materials*, 2002, **14**, 1525–1528.
14 M. Ren, Z. Zhou, Y. Li, X. P. Gao and J. Yan, *Journal of Power Sources*, 2006, **162**, 1357–1362.
15 Z. Jian, W. Han, X. Lu, H. Yang, Y.-S. Hu, J. Zhou, Z. Zhou, J. Li, W. Chen, D. Chen and L. Chen, *Advanced Energy Materials*, 2013, **3**, 156–160.
16 C. Masquelier and L. Croguennec, *Chem. Rev.*, 2013, **113**, 6552–6591.
17 K. Saravanan, C. W. Mason, A. Rudola, K. H. Wong and P. Balaya, *Advanced Energy Materials*, 2013, **3**, 444–450.
18 S.-C. Yin, H. Grondey, P. Strobel, H. Huang and L. F. Nazar, *J. Am. Chem. Soc.*, 2003, **125**, 326–327.
19 C. W. Mason and F. Lange, *ECS Electrochem. Lett.*, 2015, **4**, A79–A82.
20 G. Li, Z. Yang, Y. Jiang, C. Jin, W. Huang, X. Ding and Y. Huang, *Nano Energy*, 2016, **25**, 211–217.
21 F. Nacimiento, M. Cabello, R. Alcántara, P. Lavela and J. L. Tirado, *Electrochimica Acta*, 2018, **260**, 798–804.
22 Y. Li, Q. An, Y. Cheng, Y. Liang, Y. Ren, C.-J. Sun, H. Dong, Z. Tang, G. Li and Y. Yao, *Nano Energy*, 2017, **34**, 188–194.
23 M. Cabello, R. Alcántara, F. Nacimiento, P. Lavela, M. J. Aragón and J. L. Tirado, *Electrochimica Acta*, 2017, **246**, 908–913.
24 J. Zeng, Y. Yang, S. Lai, J. Huang, Y. Zhang, J. Wang and J. Zhao, *Chemistry – A European Journal*, 2017, **23**, 16898–16905.
25 J. Gopalakrishnan and K. K. Rangan, *Chem. Mater.*, 1992, **4**, 745–747.
26 B. L. Cushing and J. B. Goodenough, *Journal of Solid State Chemistry*, 2001, **162**, 176–181.
27 J. Gaubicher, C. Wurm, G. Goward, C. Masquelier and L. Nazar, *Chem. Mater.*, 2000, **12**, 3240–3242.
28 Z. Jian, C. Yuan, W. Han, X. Lu, L. Gu, X. Xi, Y.-S. Hu, H. Li, W. Chen, D. Chen, Y. Ikuhara and L. Chen, *Advanced Functional Materials*, 2014, **24**, 4265–4272.
29 S.-C. Yin, H. Grondey, P. Strobel, M. Anne and L. F. Nazar, *J. Am. Chem. Soc.*, 2003, **125**, 10402–10411.
30 Z.-D. Huang, T. Masese, Y. Orikasa, T. Mori and K. Yamamoto, *RSC Adv.*, 2015, **5**, 8598–8603.
31 H. Tang, Z. Peng, L. Wu, F. Xiong, C. Pei, Q. An and L. Mai, *Electrochem. Energ. Rev.*, 2018, **1**, 169–199.
32 Z. Moorhead-Rosenberg, E. Allcorn and A. Manthiram, *Chem. Mater.*, 2014, **26**, 5905–5913.
33 W. Kaveevivitchai and A. Manthiram, *J. Mater. Chem. A*, 2016, **4**, 18737–18741.
34 W. Kaveevivitchai, A. Huq and A. Manthiram, *J. Mater. Chem. A*, 2017, **5**, 2309–2318.
35 B. H. Toby and R. B. Von Dreele, *J Appl Cryst*, 2013, **46**, 544–549.
36 C. L. Farrow, P. Juhas, J. W. Liu, D. Bryndin, E. S. Božin, J. Bloch, T. Proffen and S. J. L. Billinge, *J. Phys.: Condens. Matter*, 2007, **19**, 335219.
37 A. R. Wizansky, P. E. Rauch and F. J. Disalvo, *Journal of Solid State Chemistry*, 1989, **81**, 203–207.
38 J. Liu, X. Liu, T. Huang and A. Yu, *Int. J. Electrochem. Sci.*, 2012, **7**, 10.
39 D. W. Murphy and P. A. Christian, *Science*, 1979, **205**, 651–656.
40 F. Wu, J. T. Lee, N. Nitta, H. Kim, O. Borodin and G. Yushin, *Advanced Materials*, 2015, **27**, 101–108.
41 N. Membreño, K. Park, J. B. Goodenough and K. J. Stevenson, *Chem. Mater.*, 2015, **27**, 3332–3340.

